ChemComm

Co-assembly of Shaped Nanoparticles into a Two-Dimensional Isotropic Mesophase

Journal:	*ChemComm*
Manuscript ID	CC-COM-03-2025-001661.R1
Article Type:	Communication

ChemComm

COMMUNICATION

Co-assembly of Shaped Nanoparticles into a Two-Dimensional Isotropic Mesophase

Received 00th January 20xx,
Accepted 00th January 20xx

DOI: 10.1039/x0xx00000x

Bin Wang,[a] James L. Young,[b] Emily Infante,[c] Alexander D. Fuqua,[a] Diana Sánchez Ramírez,[d] María Elena Garcia Celis[e] and Andrea R. Tao[a]*

Binary nanoparticle superlattices (BNSLs) enable the construction of new mesomaterials by combining the properties of two nanoparticle building blocks. We demonstrate two-dimensional (2D) BNSLs from silver nanocubes and gold nanospheres, analyzing their interparticle and orientational orders. Our experimental mesophase diagram identifies an isotropic phase that serves as a transition state to others.

Binary nanoparticle superlattices (BNSLs) are formed when two nanoparticle (NP) types that possess different chemical compositions, sizes, or shapes are assembled into long-range, ordered structures in two or three dimensions. BNSLs are particularly attractive structures for the design of "matter on demand" because they are able to: i) collectively combine the properties of two NP types, and ii) exhibit richer structural diversity than single-component NP superlattices.[1] The tunability associated with BNSLs have captured significant interest for applications in electronics,[2] plasmonics,[3] luminescence,[4] catalysis,[5] and other areas where bespoke functionalities are needed.[6,7]

Towards this end, a variety of BNSL structures have been reported that resemble naturally and non-naturally occurring crystal structures. For example, Shevchenko *et al.* reported the preparation of AB_x-type superlattices by mixing monodisperse metallic, semiconducting, and magnetic NPs. They achieved BNSLs with cubic, hexagonal, tetragonal, and orthorhombic packing symmetries by varying the size, surface functionality, and molar ratios between the NP building blocks.[8] This and subsequent works on crystalline[6,9] and quasi-crystalline[10,11] BNSL structures have significantly expanded the library of multicomponent self-assembled superstructures.

NP shape is a critical parameter for the formation and functional properties of BNSLs. While spherical NPs typically assemble into lattices based on simple packing criteria,[12] non-spherically shaped NPs introduce anisotropic interparticle interactions that increase BNSL structural diversity. BNSLs combining nanospheres and nanocubes have attracted special attention due to the unique octahedral symmetry of nanocubes, which enables six-, two-, and three-fold coordination geometries with others via cube faces, edges, and corners.[13] Additionally, metallic nanocubes support localized surface plasmon resonances (LSPRs) at cube corners and edges, allowing for orientation-dependent electromagnetic coupling between neighboring nanocubes.[14]

Assembling anisotropic nanoparticles often results in 'mesophases'— a partially ordered state of matter between conventional liquid and solid crystals.[15] In a recent theoretical study, Prajwal et al. performed Monte Carlo simulations on the 2D binary assembly with hard disks and squares as building blocks. In addition to hexatic and tetratic phases similar to the periodic structures that have been experimentally observed for single-component 2D NP superlattices, they unearthed two new 2D mesophases — an isotropic phase and a mosaic phase — which have the potential to serve as transition states between well-ordered 2D BNSL structures.[16] These mesophases were accessed by regulating the molar ratio between disks and squares, as well as the area fraction of the BNSLs, which is defined as the ratio of the area covered by the building blocks (both disks and squares) to the total area. The isotropic phase, where NP building blocks are randomly oriented without significant long-range orientational order, was shown to occur at lower area fractions and was notable for its potential to condense into either the hexatic or tetratic phases depending on NP molar ratio. While researchers have experimentally observed the hexatic[17,18] and tetratic[19,20] mesophases in NP assemblies, the 2D mosaic and isotropic mesophases have not yet been experimentally realized.

Here, we study the co-assembly of two NP types with different shapes—Au nanospheres (AuNSs) and Ag nanocubes (AgNCs), both grafted with thiolated polystyrene (PSSH)

[a] *Department of NanoEngineering, University of California San Diego, La Jolla, CA 92093.*
[b] *Department of Computer Science and Engineering, University of California San Diego, La Jolla, CA 92093.*
[c] *Department of Chemistry and Biochemistry, University of California San Diego, La Jolla, California 92023*
[d] *Centro de Nanociencias y Nanotecnología, Universidad Nacional Autónoma de México, 22860 Ensenada, Baja California, Mexico*
[e] *Centro de Graduados e Investigación en Química, Instituto Tecnológico de Tijuana, Unidad Otay, Blvd. Industrial s/n, Cd Industrial, 22430 Tijuana, Baja California, Mexico*

† Footnotes relating to the title and/or authors should appear here.
Supplementary Information available: [details of any supplementary information available should be included here]. See DOI: 10.1039/x0xx00000x

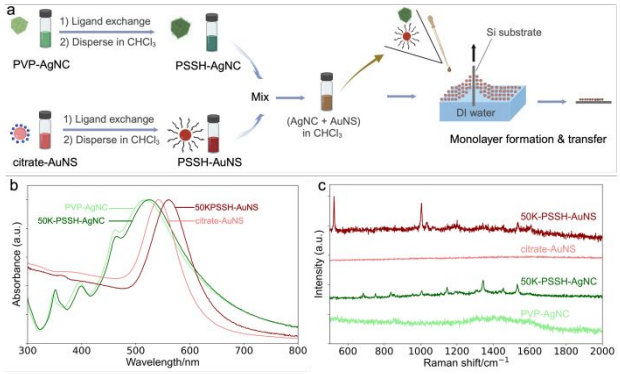

Fig. 1. (a) A schematic showing the functionalization of AgNCs and AuNSs, and the binary assembly. (b) UV-Vis of individual AgNC and AuNS nanoparticles before and after 50K-PSSH ligand exchange, with bsorbance normalized for easier comparison; (c) Raman spectra of individual AgNC and AuNS nanoparticles before and after 50K-PSSH ligand exchange, with intensity values normalized and the vertically moved for easier comparison. Noise from 865-870 cm^{-1} for 50K-PSSH-AgNC and 1214-1218 cm^{-1} for citrate-AuNS.

chains—into densely-packed 2D BNSLs with the goal of experimentally identifying an isotropic NP mesophase. Fig. 1a shows a schematic for the overall binary NP assembly process. The as-synthesized AgNCs possess an edge length of 80.3±4.0 nm and a polydispersity index (PDI) <0.1 and are natively capped with polyvinylpyrrolidone (PVP). The as-synthesized AuNSs possess a diameter of 63.5 ± 6.5 nm, a PDI < 0.1, and are natively capped with negatively charged citrate ions. The size ratio, defined as the ratio of the AuNS diameter to the AgNC edge length, was calculated to be 0.79; this was designed to be close in value with the size ratio of 0.8 predicted by Prajwal et al.[16] for hard 2D disks and squares that adopt the isotropic mesophase. Fig. 1b shows the optical extinction spectra for the individual colloidal NP dispersions obtained by UV-Vis spectroscopy before and after ligand exchange with 50K-PSSH. The spectra show a clear red shift (5 nm for AgNCs and 20 nm for AuNSs) in the UV-Vis peaks following ligand exchange, consistent with an increase in the local refractive index near the surface of the NPs observed for metal NPs that are coated with a polymer shell.[21] Fig. 1c shows the Raman spectra of dried NP samples before and after ligand exchange with 50K-PSSH. The appearance of the 1004 cm^{-1} peak attributed to the ring breathing mode of polystyrene further confirms successful PSSH functionalization on the AgNCs and AuNSs.

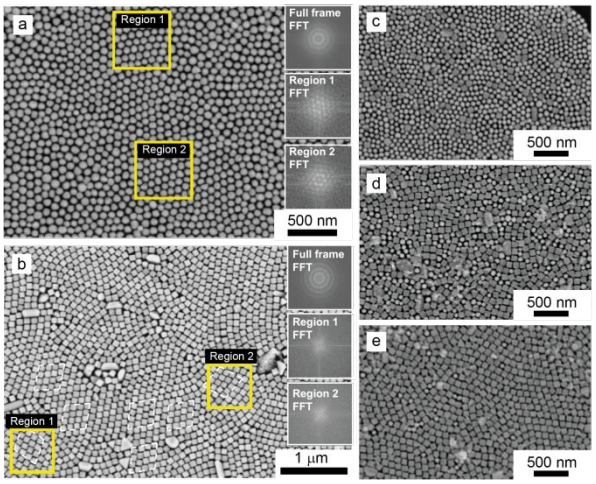

Fig. 2 (a-e) SEM images of binary assemblies from AuNS and AgNC building blocks, both capped with 50K-PSSH, and with varying AgNC molar fractions X_{AgNC} and area fractions; (a): X_{AgNC} = 0 (pure AuNS), area fraction = 0.880; (b) X_{AgNC} = 1 (pure AgNC), area fraction = 0.942; (c): X_{AgNC} = 0.126, area fraction = 0.853; (d) X_{AgNC} = 0.621, area fraction = 0.879; (e) X_{AgNC} = 0.942, area fraction = 0.913. Insets (a,b) show FFTs of full SEM frame (top), selected Region 1 (middle) and Region 2 (bottom). Rhombus (b) acute angle: 75 degrees. Scale bars: 500 nm (a,c,d,e) and 1 µm (b).

We carried out co-assembly of the AgNCs and AuNSs into 2D binary assemblies by creating a floating NP monolayer at an air-water interface using a previously described method.[22] Each PSSH-grafted NP type was dispersed in $CHCl_3$ and then mixed to generate dispersions with varying molar ratios of AgNCs (X_{AgNC}), ranging from X_{AgNC}=0 (only AuNSs) to X_{AgNC}=1 (only AgNCs).

Fig. 2 shows SEM results of co-assembly experiments carried out for mixtures of AgNCs and AuNSs functionalized with 50K-PSSH and with varying X_{AgNC}. Fig. 2a shows the SEM image at X_{AgNC}=0, where the AuNSs alone arrange into an ordered, close-packed 2D hexagonal lattice and is consistent with previous reports of PSSH-capped AuNSs.[23] Taking a fast Fourier transform (FFT) of the full SEM frame reveals a relatively high degree of polycrystallinity that is influenced by NP size and shape polydispersity. Defect NPs result in the formation of small domains (≈0.1 µm²) marked in yellow squares, where FFT spot patterns of individual domains show sixfold symmetry indicative of hexagonal packing (Fig. 2a insets). We assigned this assembly as a hexatic phase due to this sixfold orientational order.[24] Fig. 2b shows the SEM images obtained for X_{AgNC}=1, which indicate the formation of ordered, close-packed AgNC lattices with a rhombic unit cell (acute angle = 75°). These lattices are characterized by crystalline domains of various sizes, with large defect NPs segregating to the domain boundaries. We assigned this assembly as the tetratic phase due to this fourfold orientational order. Fig. 2c-e show SEM images of binary NP assemblies composed of AgNC and AuNS capped with 50K-PSSH for increasing AgNC molar fractions of X_{AgNC} =0.126, 0.621, and 0.942.

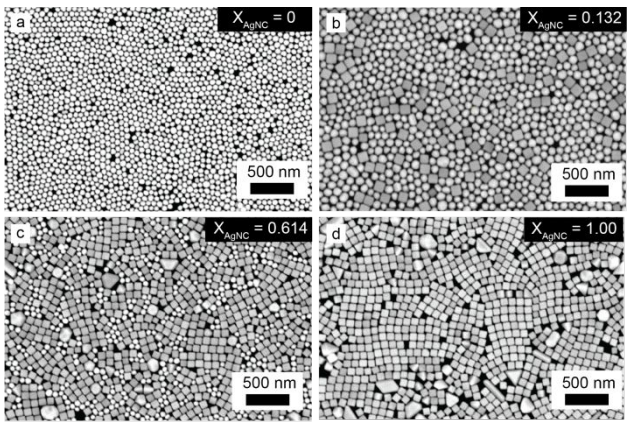

Fig 3. SEM images of binary assemblies from AuNS and AgNC building blocks, both capped with 11K-PSSH, and with varying AgNC molar fractions X_{AgNC} and area fractions; (a): X_{AgNC} = 0 (pure AuNS), area fraction = 0.828; (b) X_{AgNC} = 0.132, area fraction = 0.823; (c) X_{AgNC} = 0.614, area fraction = 0.814; (d) X_{AgNC} = 1, area fraction = 0.840. Scale bars: all 500 nm.

From SEM image analysis, we calculated the area fractions for the X_{AgNC}=0 and X_{AgNC}=1 BNSLs to be 0.880 and 0.942, respectively. Notably, these area fractions are larger than the range studied in Ref[16], which was focused on hard 2D particles with no overlap. To ensure that we were conducting experiments with the appropriate area fraction range, we also grafted AgNCs and AuNSs with a shorter 11K-PSSH and

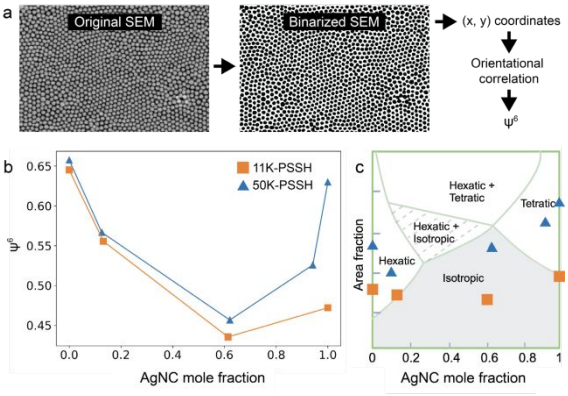

Fig. 4. (a) Flowchart of 6-fold order parameter calculation for assembly patterns using pure AuNS (Fig. 2a) as example; (b) 6-fold order parameters for binary assemblies as a function of AgNC molar ratio, calculated according to the flowchart in Fig. 2(a); and (c) Phase diagram with different assembly patterns assigned to corresponding phases.

prepared the corresponding binary assemblies with AgNC molar fractions of X_{AgNC} = 0, 0.132, 0.614, and 1 (Fig. 3). It is noteworthy that the shorter 11K-PSSH grafts results in a lower area fraction compared to longer 50K-PSSH, which is related to the weaker hydrophobicity from the shorter PSSH chain and thus less compact NP assemblies.[25] We posit that the 50K-PSSH results in low grafting density and ligands that adopt a mushroom conformation, whereas the 11K-PSSH results in a higher grafting density and ligands that adopt a more extended brush conformation, in agreement with the literature.[26,27] This is supported by dynamic light scattering measurements that reveal an average hydrodynamic radius of R_H=153 nm for 50K-PSSH AuNS and R_H=99 nm for 11K-PSSH AuNS.

To analyze superstructure order for these co-assemblies and to assign each X_{AgNC} with a corresponding mesophase (i.e. hexatic, tetratic), we calculated the 6-fold bond orientational order (ψ_6) for each assembly according to the process described in Fig. 4a. The ψ_6 values from the NP co-assemblies with different X_{AgNC} values are presented in Fig. 4b. The ψ_6 value for co-assemblies from both 50K-PSSH and 11K-PSSH grafted NPs decreases significantly with an increase in X_{AgNC}—reaching a minimum of ψ_6=0.457 at X_{AgNC} = 0.621 for 50K-PSSH and ψ_6=0.435 at X_{AgNC} =0.614 for 11K-PSSH—and then increases again. This is consistent with the observation of an isotropic phase in the Monte Carlo simulations by Prajwal *et al.*[16] where ψ_6 is expected to significantly increase upon compression/transition to the hexatic and tetratic phases. Additionally, we calculated the 4-fold orientational order (ψ_4) for the binary assemblies using similar SEM image analysis. Notably, ψ_4 does not show a significant increase upon isotropic compression to the hexatic and tetratic phases (Fig. S1) which closely agrees with computational predictions. Based on trends in ψ_4 and ψ_6, we assigned these two co-assemblies (X_{AgNC} = 0.621 for 50K-PSSH, X_{AgNC} =0.614 for 11K-PSSH) as isotropic mesophases. We assigned co-assemblies with higher ψ_6 values to either the hexatic and tetratic and phases, distinguished by lattice symmetry.

Fig. 4c shows our corresponding area fraction-composition mesophase diagram based on these assignments. While the mesophase diagram from Prajwal *et al.* predicts several condensed mesophases — including crystalline hexagonal and square solids, as well as partially-ordered hexatic and tetratic phases[16]— we simplified our mesophase diagram by only designating a larger hexatic phase (to encompass the crystalline hexagonal solid and partially ordered hexatic phases) as well as a larger tetratic phase (to encompass the crystalline square solid and partially ordered tetratic phases). Strikingly, at X_{AgNC} = 1 for 11K-PSSH, the assembly possesses a significantly lower order value (ψ_6=0.472) than for the corresponding 50K-PSSH assembly, indicating that it likely lies in the isotropic phase or at the boundary of the isotropic and tetratic phases. This is consistent with the observation by Prajwal *et al.* that lower area fraction assemblies are dominated by the isotropic phase.

Our mesophase diagram highlights the critical role of NP surface chemistry in regulating mesophase order in these NP co-assemblies. Here, the PSSH graft conformation plays a critical role in determining area fraction and, thus, mesophase order. In addition, we observe that achieving more condensed phases beyond pure hexatic and tetratic mesophases (*e.g.,* mixture phases of hexatic + tetratic) is limited by the ability to compress surface-grafted NPs to higher area fractions. This offers a potential explanation to why prior studies involving co-assembly of NSs and NCs modified with relatively large dendritic ligands observe a “masking” effect, where size and shape differences across the two NP populations do not have a pronounced effect on BNSL order, even at near-equal molar fractions.[28] In systems where the NP core is stabilized by a “soft” molecular or polymeric ligand, both size ratio and area fraction are likely to be critical determinants of whether an isotropic mesophase can be achieved.

Our experiments indicate that NP ligands such as polymer grafts offer an additional route to control the mesostructure of binary NP assemblies and further research is needed to increase our understanding of how the explicit compression, extension, and the interdigitation of such ligands can frustrate or skew hard-particle packing. Future work will refine the size and shape uniformity for nanoparticle building blocks, prepare nanoparticle assembly on a larger scale, and explore the potential for the isotropic mesophase observed here to serve as a mesophase transition state, with the potential to lead to dynamic nanostructured materials that respond to external drivers such as pressure. Prospective applications for such binary assemblies could benefit areas where precise control of functioning nanoparticles—and thus “matter on demand”—is pursued, including luminescence,[4] electronics[29] (such as optical switches[30,31]), and biosensing and imaging,[32] amongst others.

Conceptualization: B.W. and A.R.T. Methodology: B.W. and A.R.T. Investigation: B.W., J.L.Y., E.I., A.D.F., D.S.R., M.E.G, and A.R.T. Visualization: B.W., J.L.Y., and A.R.T. Funding acquisition:

A.R.T. Project administration: A.R.T. Supervision: A.R.T. Writing – original draft: B.W. Writing – review & editing: B.W. and A.R.T.

We thank Mengjing Wang, Xiaoxiao Wang, Yilong Zhou, and Heng Jiang for discussions, and Yu Xie, Yufei Wang, Wade Shipley, Diego Velazquez, and Andrea Santiago for experimental assistances. Some figures were created with BioRender.com. We acknowledge the use of facilities and instrumentation supported by National Science Foundation through the UC San Diego Materials Research Science and Engineering Center (UCSD MRSEC) with Grant DMR-2011924 and the San Diego Nanotechnology Infrastructure (SDNI) of UCSD, a member of the National Nanotechnology Coordinated Infrastructure, which is supported by the Grant ECCS-2025752. We thank the National Science Foundation, UCSD MRSEC DMR-2011924 for financial support.

Conflicts of interest

There are no conflicts to declare.

Data availability

The data supporting this article have been included as part of the Supporting Information.†

References

1 Y. Zhou and G. Arya, *Nat Commun*, 2022, **13**, 1–12.
2 D. V Talapin, J.-S. Lee, M. V Kovalenko and E. V Shevchenko, DOI:10.1021/cr900137k.
3 X. Ye, J. Chen, B. T. Diroll and C. B. Murray, *Nano Lett*, 2013, **13**, 1291–1297.
4 K. Deng, L. Xu, X. Guo, X. Wu, Y. Liu, Z. Zhu, Q. Li, Q. Zhan, C. Li and Z. Quan, *Small*, 2020, **16**, 2002066.
5 Y. Kang, X. Ye, J. Chen, L. Qi, R. E. Diaz, V. Doan-Nguyen, G. Xing, C. R. Kagan, J. Li and R. J. Gorte, *J Am Chem Soc*, 2013, **135**, 1499–1505.
6 T. Udayabhaskararao, T. Altantzis, L. Houben, M. Coronado-Puchau, J. Langer, R. Popovitz-Biro, L. M. Liz-Marzán, L. Vuković, P. Král, S. Bals and R. Klajn, *Science (1979)*, 2017, **358**, 514–518.
7 F. Meder, S. S. Thomas, T. Bollhorst and K. A. Dawson, *Nano Lett*, 2018, **18**, 2511–2518.
8 E. V Shevchenko, D. V Talapin, C. B. Murray and S. O'Brien, *J Am Chem Soc*, 2006, **128**, 3620–3637.
9 E. Marino, R. A. LaCour, T. C. Moore, S. W. van Dongen, A. W. Keller, D. An, S. Yang, D. J. Rosen, G. Gouget and E. H. R. Tsai, *Nature Synthesis*, 2024, **3**, 111–122.
10 M. I. Bodnarchuk, E. V Shevchenko and D. V Talapin, *J Am Chem Soc*, 2011, **133**, 20837–20849.
11 X. Ye, J. Chen, M. Eric Irrgang, M. Engel, A. Dong, S. C. Glotzer and C. B. Murray, *Nat Mater*, 2017, **16**, 214–219.
12 M. J. Murray and J. V Sanders, *Philosophical Magazine A*, 1980, **42**, 721–740.
13 B. Gao, G. Arya and A. R. Tao, *Nat Nanotechnol*, 2012, **7**, 433–437.
14 S. Y. Lee, L. Hung, G. S. Lang, J. E. Cornett, I. D. Mayergoyz and O. Rabin, *ACS Nano*, 2010, **4**, 5763–5772.
15 U. Agarwal and F. A. Escobedo, *Nat Mater*, 2011, **10**, 230–235.
16 B. P. Prajwal and F. A. Escobedo, *Phys Rev Mater*, 2021, **5**, 024003.
17 K. Bhattacharjee, S. S. Vaidya, T. Pathak, J. R. Shimpi and B. L. V Prasad, *Soft Matter*, 2023, **19**, 7271–7280.
18 J. Y. Kim, S. J. Kwon, J.-B. Chang, C. A. Ross, T. A. Hatton and F. Stellacci, *Nano Lett*, 2016, **16**, 1352–1358.
19 S. Li, J. He, S. Qiao, X. Zhang and B. Liu, *Small*, 2023, **19**, 2300642.
20 A. C. Stelson, S. J. Penterman and C. M. L. Watson, *Small*, 2017, **13**, 1603509.
21 C. Thambiliyagodage, *Current Research in Green and Sustainable Chemistry*, 2022, **5**, 100245.
22 K. L. Gurunatha, S. Marvi, G. Arya and A. R. Tao, *Nano Lett*, 2015, **15**, 7377–7382.
23 S. S. Lamarre, H. Yockell-Lelièvre and A. M. Ritcey, *J Colloid Interface Sci*, 2015, **443**, 131–136.
24 Z. Hou, Y. Zong, Z. Sun, F. Ye, T. G. Mason and K. Zhao, *Nat Commun*, 2020, **11**, 2064.
25 Z. Khoryani, J. Seyfi and M. Nekoei, *Appl Surf Sci*, 2018, **428**, 933–940.
26 X. Huang and C. B. Roth, *ACS Macro Lett*, 2018, **7**, 269–274.
27 Y. Jiao, A. Tibbits, A. Gillman, M.-S. Hsiao, P. Buskohl, L. F. Drummy and R. A. Vaia, *Macromolecules*, 2018, **51**, 7257–7265.
28 D. Jishkariani, K. C. Elbert, Y. Wu, J. D. Lee, M. Hermes, D. Wang, A. Van Blaaderen and C. B. Murray, *ACS Nano*, 2019, **13**, 5712–5719.
29 K. Deng, Z. Luo, L. Tan and Z. Quan, *Chem Soc Rev*, 2020, **49**, 6002–6038.
30 P. Ahonen, D. J. Schiffrin, J. Paprotny and K. Kontturi, *Physical Chemistry Chemical Physics*, 2007, **9**, 651–658.
31 Y. Viero, G. Copie, D. Guerin, C. Krzeminski, D. Vuillaume, S. Lenfant and F. Cleri, *The Journal of Physical Chemistry C*, 2015, **119**, 21173–21183.
32 Y. Zhao, L. Shi, H. Kuang and C. Xu, *DNA Nanotechnology: From Structure to Functionality*, 2020, 267–299.

Co-assembly of Shaped Nanoparticles into a Two-Dimensional Isotropic Mesophase

Bin Wang, James L. Young, Emily Infante, Alexander D. Fuqua, Diana Sánchez Ramírez, María Elena Garcia Celise, and Andrea R. Tao*

The data supporting this article have been included as part of the Supporting Information.